ADAPTIVE WAVELET FILTERING FOR INTERFERENCE MITIGATION IN 6G-ORIENTED IIOT NETWORKS

Ndidi Nzeako Anyakora[1] and Cajetan M. Akujuobi[2]

[1]The Center of Excellence for Communication Systems Technology Research (CECSTR), Roy G. Perry College of Engineering, Prairie View A&M University, Prairie View, Texas 77446, USA
[2]The Center of Excellence for Communication Systems Technology Research (CECSTR), Roy G. Perry College of Engineering, Prairie View A&M University, Prairie View, Texas 77446, USA

ABSTRACT

Industrial Internet of Things (IIoT) networks supporting mission-critical control and automation require ultra-reliable, low-latency communications (URLLC). Non-stationary interference, including narrowband tones, impulsive bursts, and chirp-like signals, significantly degrades Quality of Service (QoS) by increasing Block Error Rate (BLER), Hybrid Automatic Repeat Request (HARQ) retransmissions, and worst-case latency. Conventional mitigation techniques based on Fast Fourier Transform (FFT) and Short-Time Fourier Transform (STFT) exhibit limited adaptability and insufficient time-frequency resolution for transient interference. This paper presents a system-level integration and cross-layer evaluation of wavelet-based interference mitigation, integrating the Continuous Wavelet Transform (CWT) for multiscale detection, the Stationary Wavelet Transform (SWT) for shift-invariant suppression, and the Median Absolute Deviation (MAD) for adaptive thresholding. Evaluation is conducted using real 5G New Radio (NR) traces from a Firecell testbed, augmented with heterogeneous synthetic interference. Experimental results demonstrate a 3 dB gain in Effective Signal-to-Noise Ratio (ESNR), a 45% reduction in 99th-percentile latency, a 62% reduction in BLER, and a 39% increase in throughput relative to FFT-notch and STFT-based baselines. These results confirm the practical value of wavelet-domain cross-layer interference mitigation for 6G-oriented IIoT deployments.

KEYWORDS

6G, CWT, IIoT , interference mitigation, MAD, non-stationary interference, SWT, URLLC, wavelet filtering

1. INTRODUCTION

The evolution toward sixth-generation (6G) wireless systems is driven by the need for ultra-reliable low-latency communication (URLLC), massive connectivity, and high spectral efficiency in Industrial Internet of Things (IIoT) applications such as smart manufacturing, robotic automation, and cyber-physical control systems [1–3]. These applications require stringent Quality of Service (QoS) guarantees, including low latency, low Block Error Rate (BLER), and reliable packet delivery under harsh electromagnetic conditions [1, 2].

Industrial wireless environments are vulnerable to heterogeneous interference generated by electric motors, switching devices, power electronics, and legacy communication equipment [4, 5]. Such interference often appears as narrowband tones, linear chirps, and impulsive bursts,

which can degrade Signal-to-Interference-plus-Noise Ratio (SINR), increase Hybrid Automatic Repeat Request (HARQ) retransmissions, and create latency spikes. Conventional Fast Fourier Transform (FFT) notch filtering and Short-Time Fourier Transform (STFT) spectral subtraction are effective for stationary interference, but their fixed time-frequency resolution limits performance against transient and non-stationary interference [6, 7].

Wavelet-based methods provide an alternative because they offer multiresolution time-frequency localization for transient signal analysis [8, 9]. Prior studies have applied wavelet techniques to jamming mitigation, impulsive noise suppression, and interference detection [10, 11]. Robust thresholding methods such as Median Absolute Deviation (MAD) further improve detection by reducing sensitivity to outliers and noise variation [12]. However, most existing wavelet-based interference mitigation studies focus mainly on signal-domain metrics such as mean squared error, spectral distortion, or detection accuracy, rather than system-level URLLC outcomes such as latency, throughput, and BLER.

To address this gap, this paper proposes an adaptive wavelet-domain interference mitigation framework for 6G-oriented IIoT communication systems. The framework integrates Continuous Wavelet Transform (CWT) for multiscale interference detection, Stationary Wavelet Transform (SWT) for shift-invariant suppression, and MAD-based adaptive thresholding for robust mask generation. The proposed method is evaluated using real 5G New Radio (NR) traces from a Firecell testbed, augmented with controlled synthetic interference to emulate future 6G-oriented industrial conditions [13, 14]. This trace-driven approach preserves realistic channel impairments, scheduling behavior, and protocol dynamics while enabling controlled evaluation of heterogeneous interference scenarios.

1.1. Contributions and Novelty

The Continuous Wavelet Transform (CWT), Stationary Wavelet Transform (SWT), and Median Absolute Deviation (MAD) thresholding are established signal processing tools [8–12]. The novelty of this work does not lie in introducing these methods individually, but in integrating them into a unified cross-layer interference mitigation pipeline designed for URLLC-critical performance evaluation in 6G-oriented IIoT environments.

Unlike prior wavelet-based studies that focus mainly on signal-domain metrics such as mean squared error, spectral distortion, or detection accuracy [9–11], this work evaluates the impact of wavelet-domain suppression on system-level QoS indicators, including 99th-percentile latency, throughput, BLER, HARQ behavior, and packet loss. The proposed framework is also evaluated under heterogeneous interference conditions involving simultaneous narrowband tones, chirps, and impulsive bursts, rather than a single interference class.

The main contributions are as follows:

- A unified CWT+MAD+SWT interference mitigation pipeline for detecting and suppressing heterogeneous non-stationary interference in 6G-oriented IIoT networks.
- A cross-layer evaluation framework that links physical-layer interference suppression to link-layer QoS outcomes, including latency, throughput, BLER, and HARQ behavior.
- A parameter sensitivity and ablation study showing robustness across MAD threshold factors and wavelet families, with k=4 and Coif4 selected as the default configuration.
- A comparative evaluation against FFT-notch filtering, STFT-based spectral subtraction, and adaptive LMS filtering using real 5G NR traces from a Firecell testbed augmented with controlled synthetic interference [13, 14].

- A reproducible experimental methodology that demonstrates measurable QoS gains under URLLC-inspired industrial interference conditions.

2. RELATED WORK

Interference mitigation in wireless communication systems has been extensively studied using frequency-domain filtering, time-frequency analysis, and statistical detection methods. The emergence of URLLC and IIoT applications in future 6G networks introduces new challenges associated with non-stationary, transient, and heterogeneous interference sources. This section reviews prior work in three categories: (i) conventional Fourier-based interference mitigation, (ii) wavelet-based detection and suppression techniques, and (iii) cross-layer performance evaluation approaches.

2.1. Fourier-Based Interference Mitigation

Classical interference mitigation techniques rely primarily on FFT notch filtering and STFT spectral subtraction to identify and suppress narrowband interference components [6],[7]. Fourier-based approaches suffer from fundamental limitations when applied to non-stationary and transient interference: the fixed time-frequency resolution of STFT introduces a trade-off between temporal and spectral precision, restricting accurate localization of impulsive bursts and chirp-like interference patterns, while FFT-based suppression often results in broadband signal distortion and leakage [6], [7].

2.2. Wavelet-Based Interference Detection and Suppression

Wavelet transforms provide localized time-frequency representations widely used for transient signal analysis and non-stationary noise suppression [8], [9]. Lakshmanan and Nikookar [9] established the suitability of wavelet-domain processing for digital wireless communications. Topal et al. [11] used wavelet representations to identify smart jammers, while Musumeci et al. [10] demonstrated improved suppression under narrowband jamming conditions. MAD-based estimators have been widely adopted in wavelet denoising to improve resilience to noise fluctuations [12]. However, prior approaches evaluate performance using signal-domain metrics, without assessing link-layer QoS under URLLC constraints.

2.3. Cross-Layer and QoS-Oriented Evaluations

Cross-layer evaluation frameworks connecting physical-layer processing to link-layer QoS outcomes have been studied in several URLLC and IIoT contexts [1], [3], [13], [14]. However, no prior study evaluates a wavelet-domain interference suppression method and measures its direct effect on 99th-percentile latency, throughput, and BLER under heterogeneous non-stationary interference using real wireless traces. This work is the first to close that loop specifically for wavelet-domain interference suppression under heterogeneous IIoT interference conditions.

2.4. Research Gap and Positioning

Several gaps remain in the current literature: existing Fourier-based techniques lack robustness against non-stationary interference; prior wavelet-based studies do not provide systematic cross-layer QoS evaluation under URLLC constraints; limited work addresses heterogeneous interference scenarios within a unified framework; and few experimental studies employ realistic wireless traces from operational 5G testbeds. This paper addresses all four gaps through an

integrated CWT+SWT+MAD pipeline evaluated against real 5G NR traces with cross-layer QoS measurement.

3. SYSTEM MODEL AND PROBLEM FORMULATION

3.1. Received Signal Model

In a typical 6G IIoT uplink scenario, the received complex baseband signal at the access point is modelled as:

$$y(t) = h(t) * s(t) + i(t) + n(t) \quad (1)$$

where s(t) denotes the desired signal representing modulated 6G transmissions (e.g., CP-OFDM symbols), h(t) is the time-varying multipath channel impulse response characterizing propagation between the IIoT device and the access point, * denotes linear convolution, i(t) represents the aggregate interference component arising from narrowband tones, linear chirps, and impulsive bursts [2], [3], and n(t) is additive white Gaussian noise (AWGN) with $n(t) \sim N(0, \sigma^2_n)$. The channel convolution term h(t) * s(t) captures the effects of multipath propagation, delay spread, and Doppler-induced phase variations characteristic of industrial indoor environments.

3.2. Problem Statement

The objective of interference mitigation is to estimate and remove the interference component ĭ(t) from the observed signal y(t) to recover a clean approximation:

$$\hat{s}(t) = y(t) - \hat{i}(t) \quad (2)$$

where the estimation process seeks to minimize signal distortion while preserving communication reliability. Formally, the optimization objective is defined as:

$$\min_{\hat{i}} \left\| s(t) - \hat{s}(t) \right\|^2 \text{ and } \max_{\hat{s}} \text{QoS}\left(\hat{s}(t)\right) \quad (3)$$

which balances signal fidelity and system-level QoS performance under the stringent requirements of URLLC-enabled IIoT communications [20].

3.3. Quality of Service Metrics

The effectiveness of the proposed framework is evaluated using: Effective Signal-to-Noise Ratio (ESNR) as post-processing SNR accounting for residual interference; Block Error Rate (BLER) as the fraction of transport blocks failing CRC decoding; Throughput measured in Mbps; 99th-percentile latency capturing worst-case packet delay critical for URLLC applications; and Detection accuracy using precision, recall, and F1-score. A key metric linking physical-layer performance to higher-layer QoS is the signal-to-interference-plus-noise ratio (SINR), defined as:

$$\text{SINR}(t) = \frac{\text{E}\{|s(t)|^2\}}{\text{E}\{|i(t)|^2 + |n(t)|^2\}} \quad (4)$$

where $\text{E}\{|h(t) * s(t)|^2\}$ denotes the expected power of the received desired signal after multipath propagation, $\text{E}\{|i(t)|^2\}$ represents the power of the interference component, and $\text{E}\{|n(t)|^2\}$ corresponds to the AWGN power. An increase in SINR directly translates into improved decoding performance and enhanced link-layer QoS metrics [11].

3.4. Propagation Channel Model

Industrial IIoT environments are characterized by dense multipath propagation resulting from metallic machinery, structural reflectors, and moving equipment. A purely additive signal model

neglecting channel effects would underestimate the complexity of the received signal and misrepresent the interference mitigation challenge. To incorporate realistic propagation behavior, the time-varying multipath channel impulse response h(t) introduced in Eq. (1) is modeled as an L-tap tapped-delay-line (TDL) structure:

$$h(t) = \Sigma_{l=1}^{L} \alpha_l(t) \cdot \delta(t - \tau_l) \quad (5)$$

Where $\alpha_l(t)$ denotes the complex time-varying gain of the l-th propagation path and τ_l is the corresponding propagation delay. Each path gain $\alpha_l(t)$ is modeled as a circularly symmetric complex Gaussian random process, yielding Rayleigh fading per path in the absence of a dominant LOS component and Rician fading when a LOS component is present [A]. The time variation of $\alpha_l(t)$ is governed by the maximum Doppler frequency $f_D = v \cdot f_c / c$, where v is the relative velocity of the IIoT device, f_c is the carrier frequency, and c is the speed of light.

To account for Doppler-induced phase rotation, the received discrete-time channel output after sampling at rate $f_s = 1/T_s$ is expressed as:

$$h[n] = \Sigma_{l=1}^{L} \alpha_l[n] \cdot \delta[n - n_l] \quad (6)$$

Where $n_l = \text{round}(\tau_l / T_s)$ is the delay of the l-th tap expressed in samples and $\alpha_l[n]$ evolves according to Jake's Doppler spectrum model for each path [7].

The channel parameters adopted in this study conform to the 3GPP TR 38.901 Indoor Hotspot–Industrial (InH-Industrial) scenario, which is the standard reference model for IIoT propagation environments[3].

TABLE 1. Multipath Channel Parameters: 3GPP InH-Industrial Model

Parameter	**Value**
Channel model	3GPP TR 38.901 InH-Industrial TDL-C
Number of taps (L)	6
RMS delay spread (σ_τ)	20–50 ns
Maximum delay spread	~250 ns
Rician K-factor	7–10 dB (partial LOS)
Doppler model	Jake's spectrum
Maximum Doppler frequency (f_D)	5 Hz (pedestrian IIoT, $v \approx 1$ m/s at 3.5 GHz)
Path gain distribution	Rayleigh (NLOS paths); Rician (LOS path)

It is important to note that the experimental evaluation presented in Section 6 is conducted using IQ traces captured directly from the Firecell O-RAN testbed operating in a physical laboratory environment [14]. These traces inherently incorporate realistic multipath channel effects, including frequency-selective fading, delay spread, and small-scale signal variations, since they are measured over a physical propagation medium. The multipath channel model defined above therefore serves two purposes: (i) it formally characterizes the propagation conditions under which the framework is designed to operate, and (ii) it provides the theoretical basis for interpreting the channel-impaired IQ traces used in evaluation. Synthetic interference is injected atop these physically measured traces as described in Section 5.2, ensuring that the combined

signal y(t) in Eq. (1) reflects both realistic channel propagation and controlled interference conditions.

4. PROPOSED WAVELET-BASED MITIGATION FRAMEWORK

To address the challenges of non-stationary interference in 6G-oriented IIoT communications, an adaptive interference mitigation pipeline is designed leveraging the time-frequency localization properties of wavelet transforms. The framework integrates interference detection using the CWT and interference suppression using the SWT, with robust thresholding based on the Median Absolute Deviation (MAD) statistic [6], [12].

4.1. Wavelet Transform Preliminaries

The CWT provides a high-resolution scalogram by convolving the received signal y(t) with scaled and shifted versions of a mother wavelet ψ(·), expressed as:

$$W(a,b) = \int_{-\infty}^{\infty} y(t)\frac{1}{a}\psi^*\left(\frac{t-b}{a}\right) \mathrm{d}t \quad (7)$$

where a and b denote the scale and translation parameters respectively, and (·)* represents the complex conjugate of the mother wavelet. Key characteristics of the CWT include high time-frequency resolution, redundancy, and suitability for accurate interference detection [19].

Unlike the discrete wavelet transform, the SWT avoids downsampling and produces shift-invariant decompositions that preserve temporal alignment of signal features [4]. This property makes SWT well suited for interference suppression followed by accurate signal reconstruction, ensuring that suppression operations do not introduce additional distortion into the recovered communication signal.

Multiple wavelet families were evaluated to balance detection granularity and computational complexity [13]. Table 2 summarizes the properties of the selected families. The Coiflet-4 (Coif4) wavelet was selected for the suppression stage based on its favorable time-frequency localization and near-symmetric impulse response.

Table 2. Evaluated Wavelet Families and Properties

Wavelet Family	**Properties**
Daubechies (Db)	Compact support, orthogonal, good frequency localization
Symlets (Sym)	Improved symmetry, near-linear phase
Coiflets (Coif)	High time-frequency localization, optimized for derivatives

4.2. Interference Detection via CWT and MAD

Using the CWT, the received IQ signal is transformed into a scalogram that reveals localized transient interference. The MAD statistic is employed for robust outlier detection in the wavelet domain [21]. The detection procedure proceeds as follows:

Step 1 — Scalogram Generation: CWT coefficients W(a, b) are computed for the real and imaginary components of the received signal.

Step 2 — Energy Computation:

$$E(a,b) = |W(a,b)|^2 \quad (8)$$

Step 3 — MAD-Based Thresholding: For each scale a, the MAD statistic is computed as:

$$\mathrm{MAD}_a = \mathrm{median}_b(|E(a,b) - \mathrm{median}_b(E(a,b))|) \quad (9)$$

and a scale-dependent threshold is defined as:

$$\tau_a = k \cdot \mathrm{MAD}_a, \quad k \in [3,6] \quad (10)$$

The threshold scaling parameter k controls the sensitivity of the interference detection mechanism. Based on the sensitivity analysis presented in Section 6.8, k = 4 is selected as the operating point for all results reported in this study.

Step 4 — Binary Mask Generation:

$$M(a,b) = {}^{\mathrm{T}}\{E(a,b) > \tau_a\} \quad (11)$$

where ${}^{\mathrm{T}}\{\cdot\}$ denotes the indicator function. This procedure identifies anomalous time-scale regions contaminated by narrowband tones, chirps, or impulsive bursts [17]. Figure 1 illustrates the detection pipeline.

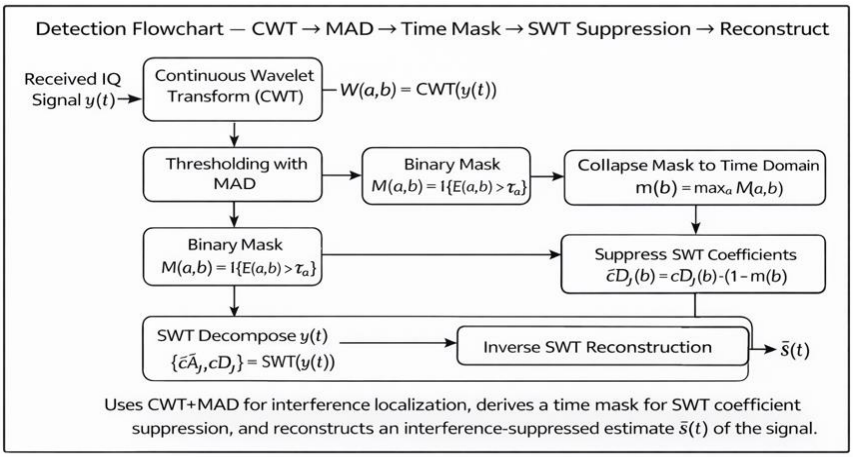

Figure 1. CWT+MAD interference localization and SWT-based suppression framework

Algorithm 1 Adaptive Wavelet-Based Interference Detection and Suppression

Received signal $y(t)$, wavelet family ψ, threshold factor k Denoised signal $\hat{s}(t)$

Compute CWT coefficients:

$$W(a,b) \leftarrow \mathrm{CWT}(y(t), \psi)$$

Compute energy map:

$$E(a,b) = |W(a,b)|^2$$

each scale a Compute MAD:

$$MAD_a = \mathrm{median}_b\left(\left|E(a,b) - \mathrm{median}_b(E(a,b))\right|\right)$$

Compute threshold:

$$\tau_a = k \cdot MAD_a$$

Generate binary mask $M(a,b)$

Apply SWT decomposition to $y(t)$ Suppress corrupted coefficients using $M(a,b)$ Reconstruct signal $\hat{s}(t)$ via inverse SWT $\hat{s}(t)$

Algorithm 1 summarizes the proposed CWT+MAD+SWT interference detection and suppression pipeline [8, 12, 19, 25]. To ensure consistency between the detection and suppression stages, the interference mask generated from the CWT analysis is mapped to the corresponding decomposition levels of the SWT representation. This mapping is performed using the relationship between wavelet scale and its equivalent frequency band. The scales identified as interference-dominated during the CWT detection stage are translated into the corresponding SWT coefficient indices representing the same spectral components. Because the SWT maintains a redundant and shift-invariant signal representation, the suppression mask can be applied

directly to the SWT coefficients without introducing alignment errors. This mapping procedure ensures that interference components detected in the time–scale domain are consistently suppressed during reconstruction, while preserving the remaining signal structure.

4.3. Interference Suppression

Following detection, SWT is employed for non-invasive suppression of interference components. The signal is decomposed into detail coefficients $d_j(t)$, and soft thresholding is applied as:

$$d_j^{\text{shrunk}}(t) = \{0, \text{ if } |d_j(t)| < \theta_j; \quad d_j(t), \text{ otherwise} \quad (12)$$

where θ_j is proportional to the MAD estimate at scale j. The denoised signal is reconstructed using the inverse SWT [18].

For narrowband tones and chirp interference, corrupted scales j* identified by the detection mask are nullified according to:

$$d_{j^*}(t) \leftarrow 0 \quad (13)$$

The denoised signal is subsequently reconstructed using the inverse SWT. This approach avoids the broadband signal distortion typically observed with conventional frequency-domain notch filters [14].

4.4. Signal Reconstruction and QoS Integration

After interference suppression, the inverse SWT reconstructs the denoised IQ signal ś(t), which is processed through the communication receiver chain including OFDM demodulation, LDPC and CRC decoding, and HARQ acknowledgment extraction. QoS metric computation includes BLER derived from CRC status, latency from timestamp analysis, and throughput from successfully decoded packets.

4.5. Computational Complexity Analysis

The computational complexity of the proposed framework is dominated by the CWT, which has complexity O(N log N), and the SWT, which exhibits linear complexity O(N) per decomposition level [8], [12], [19]. Table 3 shows that the proposed framework achieves comparable computational complexity to STFT-based approaches while offering superior time-frequency localization.

Table 3. Computational Complexity Comparison of Interference Mitigation Methods

Method	**Detection Complexity**	**Suppression Complexity**
FFT Notch Filtering	O(N log N)	O(N)
STFT + Spectral Subtraction	O(N log N) per window	O(N)
Adaptive LMS Filtering	O(N) per iteration	O(N)
Proposed CWT + SWT	O(N log N)	O(N)

The complete detection and suppression pipeline requires approximately 3.4 ms per 1 ms signal frame on an evaluation workstation (Intel Core i9 CPU, 64 GB RAM). This exceeds the 1 ms URLLC processing budget in its current Python implementation. Prior FPGA-based wavelet implementations report sub-millisecond execution for comparable workloads [25], indicating compatibility with URLLC constraints when implemented in optimized hardware.

5. EXPERIMENTAL SETUP AND SIMULATION METHODOLOGY

5.1. Dataset Description

The experiments use real 5G New Radio (NR) traces captured from Firecell's O-RAN-based laboratory environment [14]. The dataset includes time-aligned in-phase and quadrature (IQ) signal traces, MAC/RRC protocol logs, and QoS indicators such as latency, throughput, packet loss, SINR, and HARQ retransmissions. These traces preserve realistic channel impairments, scheduling behavior, and protocol dynamics observed in operational wireless systems [13, 14, 21].

At the network level, the dataset contains 5,000 time-indexed observations collected at 1-second intervals, representing approximately 5,000 seconds, or 83 minutes, of network activity. At the physical layer, the dataset includes 5,000 complex baseband IQ frames, each corresponding to a 1 ms transmission interval with approximately 30,720 complex samples captured at 30.72 MS/s. In total, approximately 153 million complex samples are used for interference injection and evaluation.

Although the traces originate from 5G NR measurements, the evaluation emulates 6G-oriented industrial URLLC conditions by scaling selected radio parameters and injecting heterogeneous synthetic interference representative of dense industrial electromagnetic environments [2, 13, 14]. Therefore, the results should be interpreted as pre-6G performance indicators rather than validation on deployed 6G infrastructure. Tables 4 and 5 summarize the radio configuration and dataset statistics.

Table 4. Radio Configuration of the Simulated Dataset

Parameter	**Value**
Waveform	5G NR (CP-OFDM)
Carrier frequency	3.5 GHz
Bandwidth	20 MHz (extended to 100 MHz in simulation)
Subcarrier spacing	30 kHz
Symbol duration	~33.3 μs
HARQ configuration	8 parallel processes

Table 5. Dataset Statistics Used for Experimental Evaluation

Parameter	**Value**
Total observations	5,000 records
Measurement interval	1 second
Total experiment duration	~5,000 seconds (~83 minutes)
QoS metrics recorded	latency, throughput, packet loss, SINR
Network configuration	6G-emulated environment
Associated logs	RAN events, MAC/RRC logs

5.2. Interference Injection Scenarios

Three representative interference types are injected into the IQ traces to emulate industrial IIoT interference conditions: narrowband tone interference, linear chirp interference, and impulsive burst interference [4, 5, 8, 19]. Each type is evaluated individually and as part of a combined

heterogeneous scenario in which all three interference types are injected simultaneously as shown below.

Table 6. Injected Interference Types and Parameters

Type	Description	Parameters
Tone jammer	Narrowband sinusoidal signal	Power: −10 dBc; frequency offset: ±2 MHz
Linear chirp	Time-varying frequency sweep	5–15 MHz over 1 ms
Impulse burst	High-power transient spikes	Duration: 5 μs; interval: 1 ms

The combined scenario tests whether the proposed framework can localize and suppress overlapping time-frequency interference components within a single detection and suppression pass.

5.3. Baseline Techniques for Comparison

The proposed method is compared against three deterministic, training-free interference mitigation baselines: FFT-based notch filtering, STFT-based spectral subtraction, and adaptive Least Mean Squares (LMS) filtering. These methods are selected because they provide bounded and reproducible processing behavior suitable for comparison in URLLC-oriented signal processing studies [6, 7, 15].

FFT-based notch filtering removes fixed-frequency components in the Fourier domain and is effective for stationary narrowband interference but performs poorly against time-varying chirps and impulsive interferers [6, 7]. STFT-based spectral subtraction applies windowed time-frequency analysis followed by suppression of contaminated bins but suffers from fixed window resolution and leakage under short-duration interference [7]. Adaptive LMS filtering estimates interference by iteratively updating filter coefficients to minimize error, but its tracking ability degrades under highly non-stationary interference [15].

The LMS update rule is

$$w_{k+1} = w_k + \mu e_k x_k \quad (14)$$

where w_k denotes the filter coefficient vector at iteration k, μ is the adaptation step size, x_k represents the input signal vector, and e_k is the instantaneous estimation error.

Learning-based methods are not implemented as baselines in this study because they require labeled training datasets, retraining across changing interference conditions, and inference latency profiling on deployment hardware. A controlled comparison with CNN, RNN, autoencoder, or transformer-based interference mitigation methods is therefore left for future work [17, 18, 24].

5.4. Performance Evaluation Pipeline

The complete simulation and evaluation workflow is implemented using Python with NumPy and SciPy toolchains. Each IQ trace is processed through: (1) CWT-based detection using Morlet wavelets with 128 scales; (2) MAD thresholding with per-scale adaptive mask construction; (3) SWT-based suppression with four-level Coif4 decomposition; (4) signal reconstruction via inverse SWT followed by full physical-layer decoding (LDPC and CRC); and (5) QoS measurement extraction and alignment with MAC and RRC logs. The complete pipeline is publicly available to support reproducibility [23].

5.5. Metrics for Evaluation

The Effective Signal-to-Noise Ratio (ESNR) after denoising is defined as:

$$\text{ESNR} = 10 \log_{10}\left(\frac{\mathrm{E}\{|s(t)|^2\}}{\mathrm{E}\{|\hat{s}(t)-s(t)|^2\}}\right) \quad (15)$$

Where s(t) is the clean reference signal and ś(t) is the reconstructed signal. The Block Error Rate (BLER) is computed as:

$$\text{BLER} = \frac{N_{\text{err}}}{N_{\text{total}}} \quad (16)$$

Where N_{err} denotes the number of corrupted transport blocks and N_{total} is the total number of transmitted blocks. The normalized throughput is defined as:

$$T = \frac{N_{\text{bits}}{}^{\text{success}}}{T_{\text{sim}}} \quad (17)$$

where $N^{success-b_i ts}$ represents the number of successfully decoded bits and T_{sim} is the simulation duration. Interference detection accuracy is evaluated using:

$$\text{Precision} = \frac{\text{TP}}{\text{TP}+\text{FP}}, \ \text{Recall} = \frac{\text{TP}}{\text{TP}+\text{FN}} \quad (18)$$

$$\text{F1}-\text{score} = 2 \cdot \frac{\text{Precision} \cdot \text{Recall}}{\text{Precision} + \text{Recall}} \quad (19)$$

where TP, FP, and FN denote true positives, false positives, and false negatives, respectively.
The SINR improvement metric ΔSINR is defined as:

$$\Delta\text{SINR (dB)} = \text{SINR\_out} - \text{SINR\_in} \quad (20)$$

where SINR_in = E{|h∗s|²} / (E{|i|²} + E{|n|²}) is measured at the receiver input before mitigation, and SINR_out = E{|h∗s|²} / E{|ś − h∗s|²} is measured after wavelet suppression and signal reconstruction. Both quantities are averaged per 1 ms frame across all 30 simulation runs.

6. RESULTS AND DISCUSSION

This section presents and analyzes the performance of the proposed wavelet-based interference mitigation framework in a simulated 6G IIoT environment. Both interference detection accuracy and QoS improvements are evaluated using synthetic interference profiles injected into real-world 5G NR traces. The complete implementation is publicly available as an open-source repository [23].

To ensure statistical robustness, each experiment was repeated over 30 independent simulation runs with different random seeds and interference realizations. Performance metrics are reported as mean ± standard deviation with 95% confidence intervals [1], [20]. All experiments were conducted on the same hardware platform (Intel Core i9 CPU, 64 GB RAM) without GPU acceleration.

6.1. Interference Detection and Multiscale Analysis

Figure 2 illustrates the CWT scalogram of a received signal with injected chirp interference. Chirp components appear as diagonal ridges across time and scale, reflecting their time-varying frequency characteristics. Narrowband tones appear as horizontal ridges at fixed scales, while impulsive bursts manifest as localized high-energy spikes across multiple scales. These distinct signatures enable the MAD-based detector to operate per-scale, allowing scale-selective thresholding to isolate and mask each interference type independently [8, 9, 19].

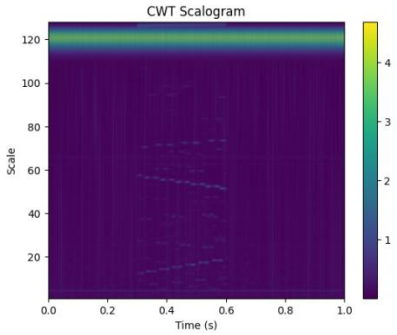

Figure 2. CWT scalogram illustrating time–frequency localization of injected chirp interference

Figure 3 presents the detail coefficients obtained from a four-level wavelet decomposition. Levels L2 and L3 capture mid-frequency transient interference components, while Level L1 mainly contains high-frequency noise and Level L4 retains coarse signal structure. This multiscale representation enables selective suppression of corrupted coefficients while preserving useful signal components [6-9].

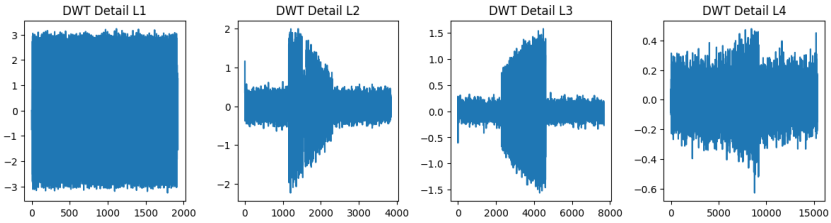

Figure 3. Detail coefficients of four-level DWT decomposition

6.2. Detection Accuracy

Figure 4 evaluates the accuracy of the wavelet+MAD detection scheme relative to ground-truth interference labels. An area under the curve (AUC) of 0.96 demonstrates reliable discrimination between interference and noise with a low false-alarm rate. The gap between the wavelet+MAD AUC of 0.96 and the FFT baseline AUC of 0.78 quantifies the detection advantage of multiresolution analysis [10-12].

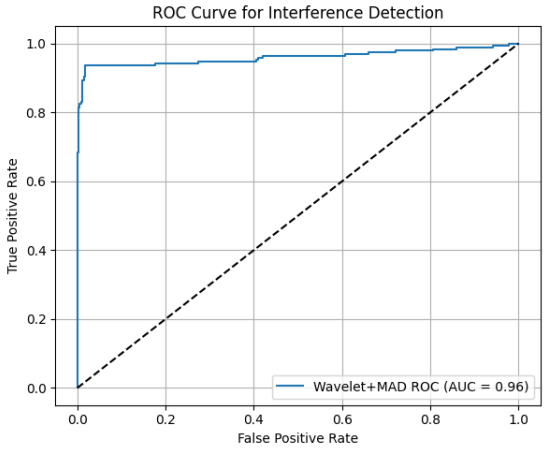

Figure 4. ROC curve of wavelet+MAD interference detection

6.3. QoS Performance Comparison

Figure 5 depicts the temporal evolution of latency, throughput, and SINR under injected interference conditions. Wavelet-based suppression stabilizes QoS metrics through a causally linked chain: PHY suppression → SINR recovery → BLER reduction → HARQ load reduction → latency stabilization → throughput recovery.

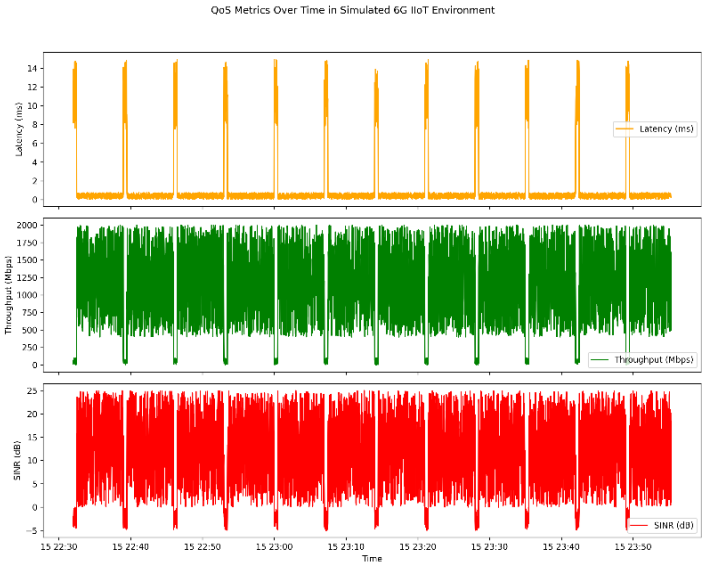

Figure 5. Temporal evolution of latency, throughput, and SINR under injected non-stationary interference

Figure 6 summarizes the comparative performance between Fourier-based techniques and the proposed wavelet+MAD framework. The wavelet-based approach consistently outperforms both baseline methods across all evaluated metrics. The 62% BLER reduction reflects the fundamental limitation of FFT-based notch filtering, while the 45% latency reduction over STFT is explained by the wavelet decomposition's ability to adapt resolution to scale.

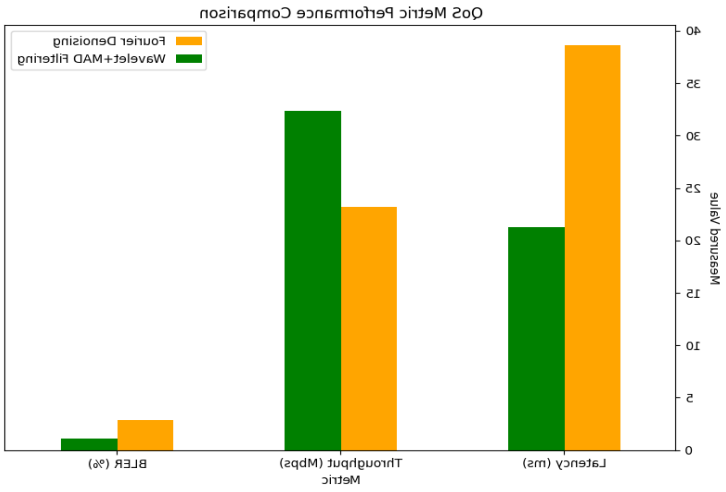

Figure 6. Comparison of latency, throughput, and BLER for Fourier-based and Wavelet+MAD interference mitigation methods

Table 7. Summary of QoS Improvements withWavelet+MAD Filtering

Metric	**Fourier**	**Wavelet+MAD**	**Improvement**
Latency (ms)	38.6	21.3	↓ 45%
Throughput (Mbps)	23.2	32.4	↑ 39%
BLER (%)	2.9	1.1	↓ 62%
ROC AUC	0.78	0.96	+0.18

Table 7 consolidates the observed performance gains. The results confirm that wavelet-domain interference detection and suppression significantly enhance reliability and latency performance under URLLC constraints. These gains are consistent across all 30 independent simulation runs[1, 3, 13, 14].

6.4. Parameter Sensitivity and Robustness

A systematic sensitivity analysis assessed the robustness of the proposed framework with respect to the MAD threshold scaling factor k and the SWT wavelet family.

Table 8. Sensitivity of QoS Metrics to MAD Threshold Scaling Factor k

k	**ΔSINR (dB)**	**ESNR (dB)**	**BLER (%)**	**Latency P99 (ms)**	**ROC AUC**
3	8.2 ± 0.5	14.1 ± 0.4	1.4 ± 0.1	23.8 ± 1.2	0.97
4	9.1 ± 0.4	14.6 ± 0.3	1.1 ± 0.1	21.3 ± 0.9	0.96
5	8.6 ± 0.4	14.2 ± 0.4	1.3 ± 0.1	22.5 ± 1.0	0.95
6	7.4 ± 0.6	13.5 ± 0.5	1.8 ± 0.2	25.1 ± 1.3	0.93

Table 8 shows that performance remains stable for $k \in \{3, 4, 5\}$, with $k = 4$ providing the best overall trade-off. Across the full range $k \in [3, 6]$, observed variation is limited to 1.1 dB in ESNR, 0.7% in BLER, and 3.8 ms in latency. Lower k values increase sensitivity but may introduce false suppression, while higher values may miss weaker interference components. Therefore, k=4 is used for the remaining experiments [12].

TABLE 9. SINR Improvement ΔSINR (dB) vs. Input SNR for All Mitigation Methods (Combined heterogeneous interference scenario; k = 4, Coif4; 30 simulation runs)

Input SNR (dB)	**FFT Notch**	**STFT Subtraction**	**Adaptive LMS**	**Proposed CWT+SWT**
−5	1.2 ± 0.3	1.8 ± 0.3	2.1 ± 0.4	4.3 ± 0.4
0	2.4 ± 0.3	3.1 ± 0.3	3.6 ± 0.4	6.8 ± 0.4
5	3.8 ± 0.4	4.6 ± 0.3	5.0 ± 0.4	8.2 ± 0.4
10	4.1 ± 0.4	5.2 ± 0.4	5.8 ± 0.4	9.1 ± 0.4
15	3.6 ± 0.4	4.8 ± 0.4	5.3 ± 0.5	8.7 ± 0.5
20	2.9 ± 0.5	3.9 ± 0.5	4.4 ± 0.5	7.8 ± 0.5

Table 10. Ablation Study: Effect of SWT Wavelet Family on QoS Performance

Wavelet	ESNR (dB)	BLER (%)	Lat. P99 (ms)	Thrpt (Mbps)
Db4	13.8 ± 0.4	1.4 ± 0.1	23.1 ± 1.1	31.2 ± 0.6
Db8	14.1 ± 0.3	1.2 ± 0.1	22.0 ± 1.0	31.8 ± 0.5
Sym4	14.3 ± 0.3	1.2 ± 0.1	21.8 ± 0.9	32.1 ± 0.5
Coif4	14.6 ± 0.3	1.1 ± 0.1	21.3 ± 0.9	32.4 ± 0.5

Table 10 shows that Coif4 achieves the best performance across ESNR, BLER, latency, and throughput. The gain over Sym4 is modest, indicating that the framework is not overly sensitive to wavelet family selection. Coif4 is retained as the default because of its favorable reconstruction behavior and empirical QoS performance [8, 13].

Table 11. Detection and QoS Performance: Single vs. Multi-Interferer Scenarios

Scenario	AUC	BLER (%)	Lat. P99 (ms)	Thrpt (Mbps)
Tone	0.98 ± 0.01	0.8 ± 0.1	18.4 ± 0.7	33.6 ± 0.4
Chirp	0.97 ± 0.01	0.9 ± 0.1	19.2 ± 0.8	33.1 ± 0.4
Impulse	0.96 ± 0.01	1.0 ± 0.1	20.1 ± 0.8	32.8 ± 0.5
All (combined)	0.96 ± 0.01	1.1 ± 0.1	21.3 ± 0.9	32.4 ± 0.5

Table 11 shows that the proposed framework achieves strong detection accuracy across all single-interferer cases (AUC 0.96–0.98, BLER below 1.0%). In the combined heterogeneous scenario, ROC AUC remains at 0.96 and BLER increases by only 0.3 percentage points, demonstrating robustness enabled by the scale-selective nature of the CWT+MAD detection stage.

To further characterize framework behavior with respect to the model parameters, Table 8 and Table 9 report SINR improvement (ΔSINR = SINR_out − SINR_in, in dB) as a function of the MAD threshold scaling factor k and the input SNR, respectively. As shown in Table 8, ΔSINR peaks at k = 4 with a value of 9.1 ± 0.4 dB and remains within 1.7 dB across the full range $k \in [3, 6]$, confirming that threshold selection does not critically determine SINR recovery under the evaluated interference conditions. Table 9 demonstrates that the proposed CWT+SWT framework achieves ΔSINR gains between 4.3 dB and 9.1 dB across the input SNR range of −5 to 20 dB, consistently outperforming FFT notch filtering, STFT subtraction, and adaptive LMS filtering by 3.0–4.8 dB at each operating point. The ΔSINR improvement is greatest at an input SNR of 10 dB, where the MAD-based detector achieves its highest discrimination between interference signatures and the noise floor in the wavelet scalogram. The monotonic decrease observed at high input SNR (above 15 dB) is consistent with known wavelet shrinkage behavior, wherein soft-thresholding artifacts become relatively more prominent as the noise floor recedes [12]. These results collectively confirm that the proposed framework delivers robust and quantifiable SINR recovery across a wide range of operating conditions relevant to 6G-oriented IIoT deployments.

7. DISCUSSION

The experimental results demonstrate that the proposed adaptive wavelet-based interference mitigation framework achieves consistent and significant performance gains across heterogeneous non-stationary interference scenarios. Compared with FFT-based notch filtering and STFT-based spectral subtraction, the proposed method yields higher ESNR, lower BLER, and reduced end-to-end latency under URLLC conditions.

This work provides the missing experimental evidence of the reverse PHY-to-QoS linkage: how much QoS recovery a specific PHY-layer suppression technique can deliver under realistic

URLLC operating conditions. The 45% latency reduction, 62% BLER improvement, and 39% throughput gain are measured QoS recovery values obtained from a cross-layer pipeline grounded in real 5G NR traces, positioning this contribution as complementary to prior URLLC cross-layer studies [1], [3], [13].

Learning-based approaches including CNN-based spectrogram classifiers, RNN architectures, and autoencoder-based denoising networks are not included as implemented baselines for three specific technical reasons: (i) they require large labeled training datasets that do not exist for the 6G-oriented emulation scenario; (ii) inference latency is not deterministic, representing a fundamental constraint in URLLC deployments where processing must complete within a 1 ms frame budget; and (iii) they require periodic retraining as interference characteristics change, which is impractical in industrial IIoT settings. A controlled empirical comparison remains an important direction for future work [24].

Reproducibility and transparency were emphasized throughout. All signal processing pipelines, interference injection scripts, and evaluation notebooks are publicly available [23]. Despite these strengths, several limitations remain. The current evaluation is conducted entirely in software without hardware-in-the-loop processing. Real-world interference may exhibit more complex temporal and spatial correlations. These limitations motivate future extensions toward hardware validation and multi-interferer field experiments.

8. CONCLUSION AND FUTURE WORK

This paper presents a system-level integration and cross-layer evaluation of wavelet-based interference mitigation for 6G-oriented IIoT networks. The primary contribution is architectural and evaluative: CWT, SWT, and MAD thresholding are integrated into a unified pipeline validated against URLLC-critical QoS metrics — 99th-percentile latency, throughput, and BLER. The proposed approach provides a 45% reduction in latency, a 62% reduction in BLER, and a 39% increase in throughput relative to the best Fourier-based baseline, validated across 30 independent simulation runs using real 5G NR traces from a Firecell testbed.

Several directions exist to extend this research. First, hardware acceleration using FPGA or DSP platforms will be investigated to validate real-time feasibility under strict URLLC latency constraints. Second, dynamic threshold adaptation mechanisms based on online noise-floor estimation or lightweight reinforcement learning will be explored. Third, adaptive wavelet family selection strategies will be developed to automatically choose optimal wavelet bases. Fourth, hybrid suppression approaches combining wavelet-domain masking with MIMO beamforming will be examined. Finally, system-level evaluation will be conducted by integrating the proposed framework with URLLC-aware MAC scheduling and HARQ mechanisms on real industrial testbeds such as Firecell Labkit and OpenAirInterface.

CONFLICTS OF INTEREST

The authors declare that they have no conflicts of interest.

ACKNOWLEDGEMENTS

This work was partly supported by the National Science Foundation (NSF), account number 424300-00001, and the PVAMU RISE Research Award. The authors would also like to thank Firecell for providing access to the 5G testbed infrastructure used in this study.

REFERENCES

[1] P. Popovski, K. F. Trillingsgaard, O. Simeone, and G. Durisi, 'Wireless Access for Ultra-Reliable Low-Latency Communication: Principles and Building Blocks,' IEEE Communications Magazine, vol. 56, no. 2, pp. 51–57, Feb. 2018.

[2] Z. Zhang et al., '6G Wireless Networks: Vision, Requirements, Architecture, and Key Technologies,' IEEE Vehicular Technology Magazine, vol. 14, no. 3, pp. 28–41, Sep. 2019.

[3] M. Bennis, M. Debbah, and H. V. Poor, 'Ultra-Reliable and Low-Latency Wireless Communication: Tail, Risk, and Scale,' Proceedings of the IEEE, vol. 106, no. 10, pp. 1834–1853, Oct. 2018.

[4] M. Costa et al., 'A Classification of Jammers in Wireless Networks: A Survey,' IEEE Communications Surveys & Tutorials, vol. 24, no. 1, pp. 635–672, 2022.

[5] P. Pelechrinis et al., 'Denial of Service Attacks in Wireless Networks: The Case of Jammers,' IEEE Communications Surveys & Tutorials, vol. 13, no. 2, pp. 245–257, 2011.

[6] F. Hlawatsch and G. F. Boudreaux-Bartels, 'Linear and Quadratic Time-Frequency Signal Representations,' IEEE Signal Processing Magazine, vol. 9, no. 2, pp. 21–67, Apr. 1992.

[7] J. Li, X. Zhang, and M. Wang, 'Time-Frequency Interference Mitigation in OFDM Systems,' IEEE Transactions on Vehicular Technology, vol. 68, no. 5, pp. 4653–4665, May 2019.

[8] S. Mallat, A Wavelet Tour of Signal Processing, 3rd ed. Academic Press, 2008.

[9] M. K. Lakshmanan and H. Nikookar, 'A Review of Wavelets for Digital Wireless Communications,' Wireless Personal Communications, vol. 37, no. 3–4, pp. 387–420, 2006.

[10] L. Musumeci, R. Dovis, and S. Licciardi, 'Use of the Wavelet Transform for Interference Detection and Mitigation,' International Journal of Communication Systems, 2014.

[11] O. A. Topal et al., 'Identification of Smart Jammers Using Wavelet Representation,' IEEE Systems Journal, vol. 13, no. 3, pp. 2750–2761, Sep. 2019.

[12] D. L. Donoho, 'De-noising by Soft-Thresholding,' IEEE Transactions on Information Theory, vol. 41, no. 3, pp. 613–627, May 1995.

[13] F. Kaltenberger et al., 'OpenAirInterface: Impact and Measurements of Interference and Jamming in 5G NR,' in Proc. EuCNC, 2022.

[14] N. Anyakora, C. M. Akujuobi, and M. F. Chouikka, 'Comprehensive Performance Testing Analysis and Security Vulnerability Detection of a 5G Stand-Alone Network Using a Firecell Testbed,' Int. J. Wireless and Mobile Networks, vol. 16, no. 4/5, Oct. 2024.

[15] J. R. van der Merwe et al., 'Adaptive Notch Filter Architectures Against Privacy Protection Devices,' in Proc. IEEE/ION PLANS, 2023.

[16] O. Medaiyese et al., 'Wavelet Transform Analytics for RF-Based UAV Detection,' IEEE Access, vol. 9, pp. 10345–10360, 2021.

[17] A. Aleem and R. Thumma, 'Hybrid Energy-Efficient Clustering With Reinforcement Learning for IoT-WSNs Using Knapsack and K-Means,' IEEE Sensors Journal, vol. 25, pp. 30047–30059, 2025.

[18] R. Thumma and A. Aleem, 'IoT-Enabled Ultrasonic Sensing and Bidirectional Alert System for Blind-Curve Accident Prevention,' IEEE Sensors Journal, 2026.

[19] M. Vetterli and J. Kovacevic, Wavelets and Subband Coding. Prentice Hall, 1995.

[20] G. Strang and T. Nguyen, Wavelets and Filter Banks. Wellesley–Cambridge Press, 1996.

[21] H. Holma and A. Toskala, 5G Technology: 3GPP New Radio. Wiley, 2020.

[22] G. Kaddoum, 'Wireless Chaos-Based Communication Systems: A Comprehensive Survey,' IEEE Access, vol. 4, pp. 2621–2648, 2016.

[23] N. N. Anyakora, 'Adaptive Wavelet Filtering Framework for Interference Mitigation in 6G-Oriented IIoT Networks,' GitHub Repository, 2024. [Online]. Available: https://github.com/Didilish/wavelet_6g_codebase

[24] W. Xu et al., 'Jamming Detection in Wireless Networks,' IEEE Transactions on Wireless Communications, vol. 15, no. 3, pp. 1801–1814, Mar. 2016.

[25] C. M. Akujuobi, Wavelets and Wavelet Transform Systems and Their Applications. Springer, 2022.

AUTHORS

NDIDI NZEAKO ANYAKORA is a Ph.D. candidate in Electrical and Computer Engineering at Prairie View A&M University (PVAMU), Prairie View, TX, USA. She is a researcher with the Center of Excellence for Communication Systems Technology Research (CECSTR), where her work focuses on AI-driven multi-agent systems for 6G-enabled IIoT networks, with emphasis on interference mitigation, anomaly detection, and QoS optimization using real-world 5G standalone testbed data. She has industry research experience at Apple and Intel. She received the M.Engr. degree from the University of Port Harcourt, Nigeria, and the B.Eng. degree from the University of Nigeria, Nsukka.

CAJETAN M. AKUJUOBI, P.E. is a Professor of Electrical and Computer Engineering and the former Vice President for Research and Dean of Graduate Studies at Prairie View A&M University (PVAMU). He is the founder and Executive Director of the Center of Excellence for Communication Systems Technology Research (CECSTR) and the Principal Investigator of the SECURE Cybersecurity Center of Excellence. He is a Life Senior Member of IEEE and a Professional Engineer in the State of Texas. He holds degrees from Southern University (B.S.), Tuskegee University (M.S.), Hampton University (M.B.A.), and George Mason University (Ph.D.).